


Quantum-inspired microwave phase superresolution at room temperature

Leonid Vidro¹,* Liran Shirizly¹, Naftali Kirsh, Nadav Katz¹, and Hagai S. Eisenberg¹
Racah Institute of Physics, Hebrew University of Jerusalem, Jerusalem 91904, Israel

 (Received 10 April 2023; revised 7 May 2024; accepted 29 July 2024; published 4 September 2024)

Quantum metrology has been shown to surpass classical limits of correlation, resolution, and sensitivity. It has been introduced to interferometric radar schemes, with intriguing preliminary results. Even quantum-inspired detection of classical signals may be advantageous in specific use cases. Following ideas demonstrated so far only in the optical domain, where practically no thermal background photons exist, we realize room-temperature microwave frequency super-resolved phase measurements with trillions of photons, while saturating the Cramer-Rao bound of sensitivity. We experimentally estimate the interferometric phase using the expectation value of the parity operator by two methods. We achieve superresolution up to 1200 times better than the wavelength with 25-ns integration time and 56-dB SNR.

DOI: [10.1103/PhysRevApplied.22.034008](https://doi.org/10.1103/PhysRevApplied.22.034008)

I. INTRODUCTION

In quantum metrology, nonclassical states are used in measurement devices to estimate a physical parameter with enhanced sensitivity. The parameter can be a time interval, an energy gap, or distance, but in most cases, the measurement is achieved by evaluating some phase of an oscillatory system. The most commonly used states are optical states of the electromagnetic field.

Many works have shown the quantum advantages of using squeezed light [1–5] or photonic NOON states [6–8], but as these advantages are very sensitive to losses, their use in real-world applications is severely limited. Thus, an intermediate application regime is defined as *quantum inspired* (QIN). The term QIN is used to describe new approaches to classical fields of research based on ideas that originate from the disciplines of quantum research [9–14]. In the field of sensing, this could mean that the used states are classical, but the measurement is still quantum mechanical or of a quantum mechanical observable. These approaches can have enhanced performance, but cannot exceed classical limits such as sensitivity beyond the shot noise limit (SNL). Nevertheless, they can exhibit lateral superresolution far beyond the Rayleigh limit, and saturate the classical sensitivity limit of the Cramer-Rao (CR) bound over a wide range of parameters.

Previous demonstrations of QIN-sensing applications utilized optical photons for high SNR and low background conditions [15,16]. Optical photons are advantageous as blackbody radiation background at room temperatures is negligible in this part of the electromagnetic spectrum. Extension of such ideas to the rf domain has been suggested in order to improve the sensitivity of radar

systems [17]. As photon energies in the rf frequency domain are orders of magnitude smaller than in the optical domain, room-temperature background can hinder their usefulness.

A central QIN approach, which is also behind the quantum radar proposal [18–20], is to measure the expectation value of the parity operator instead of the number operator at the output of an interferometric setup. Both theory and experiments supported the resolution enhancement as well as the optimized sensitivity that such a measurement yields. In previous works, the expectation value of the parity operator was experimentally estimated for optical fields, where single-photon detectors at room temperature are readily available, and the background temperature is effectively zero. This value was estimated by either a homodyne detection [16] or by a photon-number resolving measurement [15]. In this work, we demonstrate a parity measurement of an interferometric phase between electromagnetic waves in the rf domain, where the thermal background is at least thousands of photons, and the detection of single photons at room temperature is impossible. The idea of measuring the parity operator leads to a convenient detection scheme at the dark port of the interferometer, in contrast to the standard approach of intensity measurement, which gives the Rayleigh limit on resolution. The parity of the output field is estimated by two different methods, saturating the Cramer-Rao bound of the sensitivity while achieving a super-resolved feature. The width of this feature scales inversely proportional to the square root of the SNR allowing practical advantages in choosing the working point and in resolving phase changes. It also gives the intuitive definition of resolution as the width of the narrowest feature of the measured signal, a more useful sense of resolving changes, when taking noise into account, in contrast to the Rayleigh limit,

*Contact author: leonid.vidro@mail.huji.ac.il

which does not depend on SNR at all. This shows how a quantum-inspired approach could lead to advantages in performance and implementation even in a completely classical scenario like ours. In Sec. II, we present the theory behind the two methods. The experimental setup and the results are depicted in Secs. III and IV, respectively. We conclude with a discussion of these results in Sec. V.

II. THEORETICAL BACKGROUND

In what follows, we present a relatively brief theoretical background that includes the quantum origins of the idea. For a more detailed background, please see Appendix A. When making phase-sensitive measurements, one chooses to measure and calculate a parameter $M(\phi)$, which is susceptible to the phase. The width of the parameter's function with respect to the phase is the *resolution* of the measurement

$$\text{Res}(\phi) = \text{FWHM}(M(\phi)). \quad (1)$$

The **sensitivity** of the phase measurement is derived from the precision of the measurement ΔM and the slope of the function $M(\phi)$

$$\Delta\phi = \frac{\Delta M}{\partial M / \partial \phi}. \quad (2)$$

Thus, to have a more sensitive measurement, one would like to measure a low noise parameter and a narrow resolution feature with a steep slope.

When the noise statistics are known, the CR bound [21,22] gives the maximum possible precision of the phase measurement over various measurements and estimators. The classical limit of a phase resolution measurement is half of the used wavelength (such as the Rayleigh limit of imaging resolution), and shot noise imposes the limit for sensitivity. It was shown that the expectation value of the parity operator $\langle \hat{\Pi} \rangle$ presents superresolution for phase estimation using coherent states, saturating the shot noise limit when no thermal noise is present [18]. $\langle \hat{\Pi} \rangle$ was also shown to exhibit super-sensitivity when using quantum two-mode squeezed vacuum (TMSV) states. The parity operator is defined as

$$\hat{\Pi} = (-1)^{\hat{N}}, \quad (3)$$

where \hat{N} is the photon-number operator. Its expectation value depends on the probability P_n of measuring n photons, as well as it being proportional to the value at the origin point of the Wigner representation of the quantum state of the electromagnetic field [23] as a function of the

field quadratures

$$\langle \hat{\Pi} \rangle = \sum_{n=0}^{\infty} (-1)^n \cdot P_n = \pi \cdot W(0, 0). \quad (4)$$

For Gaussian states, the Wigner representation coincides with the classical phase-space distribution up to the uncertainty between the two quadratures, which is negligible in this experiment. The classical and quantum Fisher information and the CR bound coincide in this case as well [24]. We keep denoting the classical phase-space distribution by W for reasons of convenience and methodology.

For a single-mode symmetric Gaussian state, μ is the displacement from the origin (with some predefined reference phase). $N_c = \mu^2/2$ is the average number of photons, while σ is its uncertainty. Note that $\mu = \sqrt{2}|\alpha|$, where α is the conventional displacement of a coherent state and $|\alpha|^2 = N_c$. For a coherent state $\sigma^2 = \frac{1}{2}$ is the minimum possible quantum noise that is symmetric for both quadratures. A coherent state is also a shot-noise-limited signal. For a thermal state $\mu = 0$ and $\sigma^2 = N_{\text{th}} + \frac{1}{2}$, where N_{th} is the average number of photons of the thermal state.

For a coherent state superimposed with thermal noise in the same mode, the Wigner representation is just an appropriately scaled convolution of the representations of the two states [25,26], resulting in $\mu^2/2 = N_c$ and $\sigma^2 = N_{\text{th}} + \frac{1}{2}$. We define a phase-space signal-to-noise ratio as

$$\text{SNR} = \frac{N_c}{N_{\text{th}} + 1/2}. \quad (5)$$

This value coincides with the full definition of signal-to-noise ratio when the thermal noise is much higher than the shot noise. For white noise, such as the noise in our system, the SNR scales down linearly with increased integration time. The expectation value of the parity operator of such a Gaussian state is

$$\langle \hat{\Pi} \rangle = \pi \cdot W(0, 0) = \frac{1}{2\sigma^2} e^{-\frac{\mu^2}{2\sigma^2}}. \quad (6)$$

For an interferometric phase measurement of a coherent state with N_c photons on average and a phase ϕ , the expectation value of the parity operator is

$$\langle \hat{\Pi} \rangle = \frac{1}{2N_{\text{th}} + 1} e^{-\frac{N_c \sin^2(\phi/2)}{N_{\text{th}} + 1/2}}. \quad (7)$$

The CR bound on measuring an interferometric phase ϕ for high SNR is given by

$$\Delta\phi_{\text{min}} = \sqrt{\frac{2}{\text{SNR}}} = 2 \frac{\sigma}{\mu} = \sqrt{2 \frac{N_{\text{th}} + 1/2}{N_c}}, \quad (8)$$

which is reduced to the shot noise limit when $N_{\text{th}} = 0$.

A direct measurement of the parity is not always available. In fact, sometimes estimating the mean value of the parity from the number of photons is better than from parity values (since the parity value has less information than the number of photons).

By measuring the field quadrature distribution in phase space, $W(0, 0)$ can be estimated using a maximum-likelihood fit. The error in this estimation can be derived from the Fisher information of the distribution. The sensitivity of the phase measurement approaches the CR bound for large values of SNR.

Another method for estimating $W(0, 0)$ [15,16] is a projection measurement on $W(0, 0)$. For a photon-number measurement, this is a projection on the vacuum state, measuring the probability that no photons arrived at all. For a phase-space measurement, this would be done by calculating the probability of the measurement being inside some phase-space area defined by a threshold radius a from the origin:

$$\tilde{W}(0, 0) \approx \frac{1}{\pi a^2} \int_0^{2\pi} d\theta \int_0^a dr r W(r, \theta). \quad (9)$$

The probability of the measurement being inside this radius is given by the cumulative distribution function (CDF) of the marginal radial distribution in the phase space up to a . For a symmetric Gaussian distribution, the marginal radial distribution is Rician.

The choice of a affects both the resolution and the sensitivity of the measurement and one can choose a working point that suits the specific requirements of the system. A smaller threshold gives a better resolution, but requires a larger number of measurements. The optimal threshold radius is on the order of σ . The best possible sensitivity with this method does not saturate the CR bound

but asymptotically approaches it up to a factor of 1.26 calculated numerically, see Appendix A3.

III. EXPERIMENTAL SETUP AND ANALYSIS

The experimental setup depicted in Fig. 1 is equivalent to an optical Mach-Zehnder interferometer. The general idea of the setup is to create a completely destructive interference between a probe signal and a reference signal—this creates a dark port at the output of an interferometer. In contrast to the standard measurement of intensity, the value of $W(0, 0)$ changes sharply when the phase of the probe signal changes. This reflects the noise of the signal rather than the wavelength as in the standard method. To measure $W(0, 0)$ a homodyne measurement is performed on the dark port and a phase-space distribution is recovered. The homodyne measurement is carried out simply by a direct Fourier transform of the dark-port signal. A signal generator is the source of the rf signal. The first beam splitter is an rf splitter-combiner, and the latter is an rf hybrid splitter-combiner [27]. At one of the arms, an IQ mixer controls the interferometric phase ϕ . The output is sampled directly by an oscilloscope, then Fourier analyzed, effectively conducting homodyne detection. The input signal is also sampled for a phase reference. A Fourier decomposition with phase relative to the reference signal gives the quadratures for a single sample of the phase-space distribution. Several sequences of the signal construct the phase-space distribution from which $\langle \hat{\Pi} \rangle$ can be estimated.

The signal frequency is 4.96 GHz, and the oscilloscope's sampling rate is 20 GS/s, well beyond the Nyquist limit. The signal frequency is adjusted to a minimum point of the system spectral noise. The sample duration of 25 ns is such that the signal frequency would be exactly on the grid of the discrete Fourier spectrum.

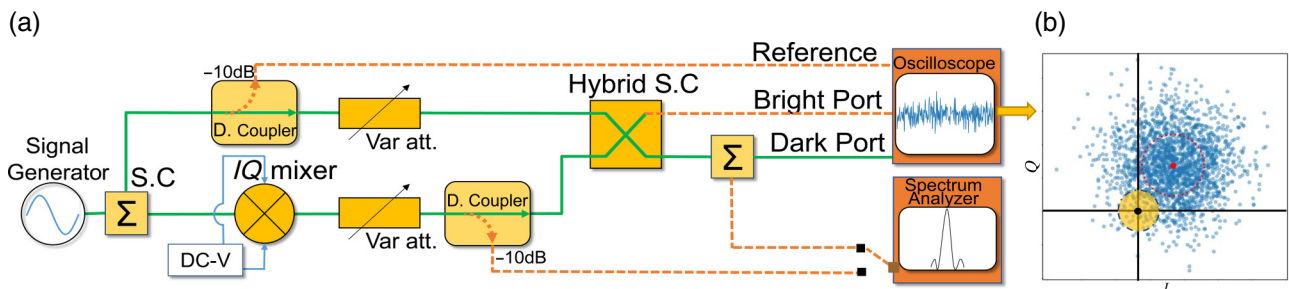


FIG. 1. (a) Experimental Mach-Zehnder-like configuration and a sample IQ distribution analysis. A signal generator is the source of a coherent signal at 4.96 GHz. A nonunitary (Wilkinson power divider) splitter-combiner splits the signal into two paths, and a unitary rf hybrid splitter-combiner interferes the two paths. The two output ports are sampled directly by an oscilloscope. An IQ mixer controls the relative phase at one arm by applying the appropriate dc voltage. A directional coupler at the upper arm provides a phase reference signal. A directional coupler at the lower arm allows the calibration of the working point of the IQ mixer using a spectrum analyzer. (b) Analysis sample: a complex FFT amplitude of each 25-ns time series is a point in phase space. The red dot and circle are the mean and standard deviation of the distribution. The yellow circle centered at the origin designates the area for the threshold analysis. See the main text for more details.

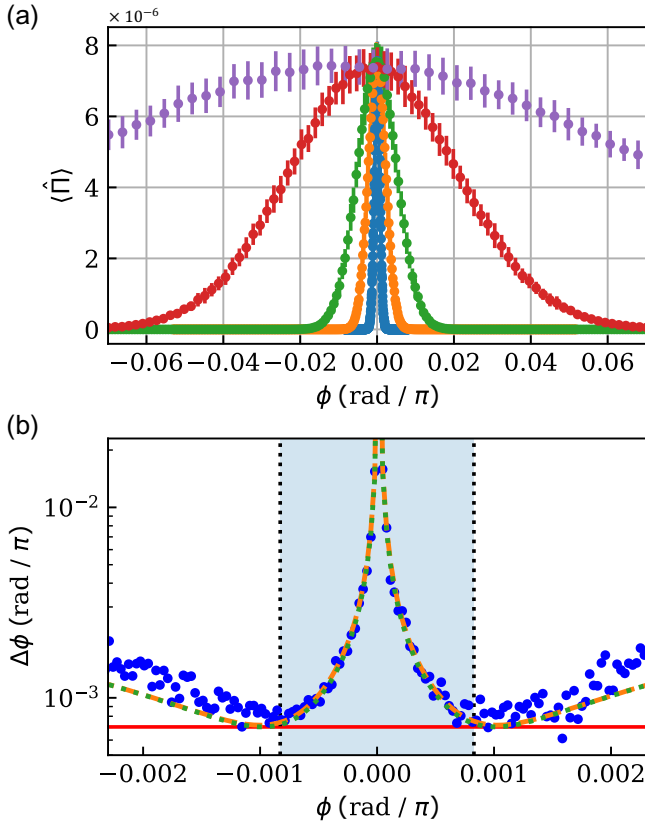


FIG. 2. Output field parity and its sensitivity, estimated by a maximum-likelihood fit. (a) Estimated parity for different SNR values, obtained by the fitting procedure: presented curves are for SNR values of 14.8, 26.3, 38.8, 45.9, and 56.1 dB, from wide to narrow trace. (b) Sensitivity around the minimal output phase, for the SNR = 56.1 dB measurement, normalized per a single 25-ns measurement. Blue dots are values derived from the measured parity, orange and green dashed lines represent the fit and theoretical calculation of the sensitivity, respectively, which are not distinguishable at this scale. The solid red line marks the Cramer-Rao bound. The blue shaded area designated the FWHM range of the parity curve.

The system was calibrated before measurements for different values of signal power. First, the dc offset of the IQ mixer was found by an automatic minimization procedure using a spectrum analyzer. Then we set port 1 of the hybrid as the dark port by the same minimization procedure. The latter procedure finds the “zero” interferometric phase and finely adjusts the amplitude to compensate for imbalances in the interferometer, including the extinction ratio of the components, resulting in an overall extinction ratio of 90 dB.

Variable digital attenuators are used in each arm in order to control the signal power. The thermal noise of the system is dominated by the oscilloscope noise. We scanned the phase for five different values of signal power approximately 10 dB apart. For each value of the interferometric

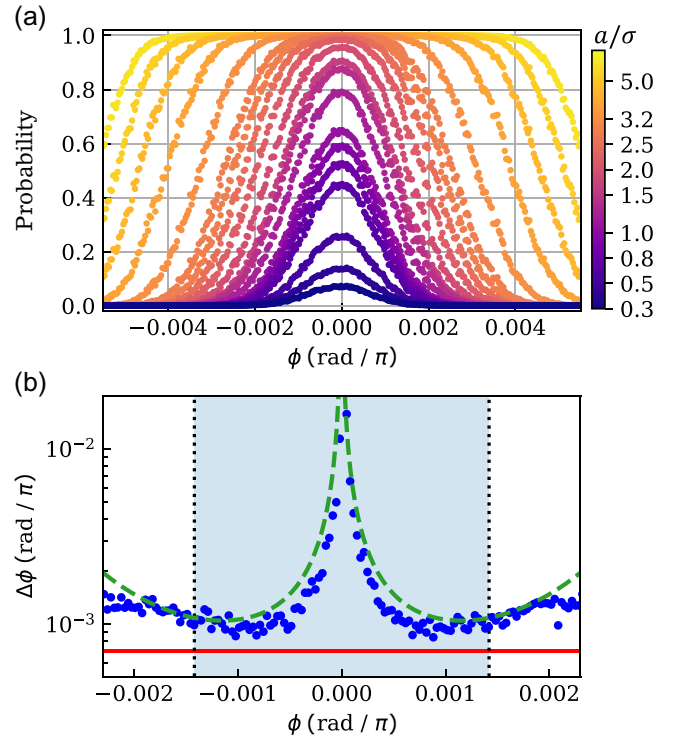


FIG. 3. Output-field resolution and its sensitivity, estimated by the threshold method. (a) The measured probability of an IQ sample within the threshold area at SNR = 56.1 dB. The color represents different ratios between the threshold a and the noise σ (b) Sensitivity plot derived from the parity measurement for SNR = 56.1 dB and threshold $a = 1.5\sigma$, normalized per a single 25-ns measurement. Blue dots are values derived from the measured parity, the green dashed line represents the theoretical calculation of the sensitivity. The solid red line marks the Cramer-Rao bound. The blue shaded area designated the FWHM range of the parity curve.

phase, at each power, the measurement was repeated 200 times to estimate the error.

The SNR of the measurement was controlled by the signal power but can be controlled also by the integration time. See Appendix B for more details.

The $W(0,0)$ value is estimated by the two methods described in Sec II; by a maximum-likelihood fit to the phase-space distribution and by using the threshold method, where $\tilde{W}(0,0)$ is evaluated by counting the number of phase-space samples within a threshold radius a . The phase-space distribution was analyzed using 200 samples. The error in estimating $W(0,0)$ scales as the square root of the number of phase-space measurements and so is the sensitivity. The presented sensitivity is normalized to a single phase-space measurement for better comparison.

IV. RESULTS

Figure 2(a) presents $\langle \hat{\Pi} \rangle$ as estimated by a maximum-likelihood fit over a range of interferometric phases, for

several values of signal power. The relevant N_c and N_{th} as well as the corresponding SNR were extracted from a fit to Eq. (7). Errors were estimated by repeating the experiment 200 times for each data point. The maximum value of $\langle \hat{\Pi} \rangle$ depends only on N_{th} , thus remaining unchanged over different values of the SNR. N_{th} was also verified independently by a direct measurement, with an agreement to the fit value of $N_{th} = 67.1 \pm 0.3 \cdot 10^3$ photons for 25-ns integration time. The FWHM of the parity measurement corresponds to the measurement resolution. The scaling of the FWHM is following $1/\sqrt{\text{SNR}}$ and the highest resolution demonstrated at 56.1 dB is 1200 times smaller than the wavelength. The same plot with a logarithmic x axis is shown in Fig. 8. Since thermal noise is white, the SNR scales down linearly with longer integration time. The resolution of the Rayleigh limit, which is achieved by the standard intensity measurement, is much larger than the values measured and therefore is not denoted in the figures.

Figure 2(b) presents the sensitivity as a function of the phase for the highest resolution, normalized per a single phase-space measurement (of 25 ns). A theoretical curve and a fit to the sensitivity are also shown, both with very good agreement with the measurement central part. The minimum of the fit saturates the CR bound.

Figure 3(a) presents parity-estimation results using the threshold method for the highest value of SNR = 56.1 dB and different values of threshold radius a . When the threshold satisfies $a \gg \sigma$, most of the phase-space points are within the threshold radius even when the phase changes. In this case, the estimated parity saturates. When $a \leq \sigma$, the resolution is better. However, many samples are required for appropriate estimation, thus making the measurement less applicable to some cases.

The choice of a affects both the resolution and the minimum possible sensitivity.

Figure 3(b) presents a sensitivity plot for SNR = 56.1 dB and $a = 1.5\sigma$. The value of a was chosen considering a trade-off between sensitivity and resolution. The sensitivity is normalized per a single phase-space measurement. For more details, see Appendix A 3.

Figure 4 presents the scaling of the resolution and the sensitivity with the SNR, for estimating $\langle \hat{\Pi} \rangle$ by the two methods. The SNR is the figure of merit defining the performance of this measurement at all regimes down to the shot noise limit. In the threshold method, a/σ is the second parameter defining the resolution and the sensitivity relative to the CR bound, in addition to the SNR value.

For both methods, the resolution and the sensitivity are of the same order of magnitude, in contrast to the classical method, where the resolution is unaffected by the SNR. Both scale as $1/\sqrt{\text{SNR}}$. The sensitivity of the estimation by the maximum-likelihood fit method saturates the CR bound and the threshold method reaches the bound up to

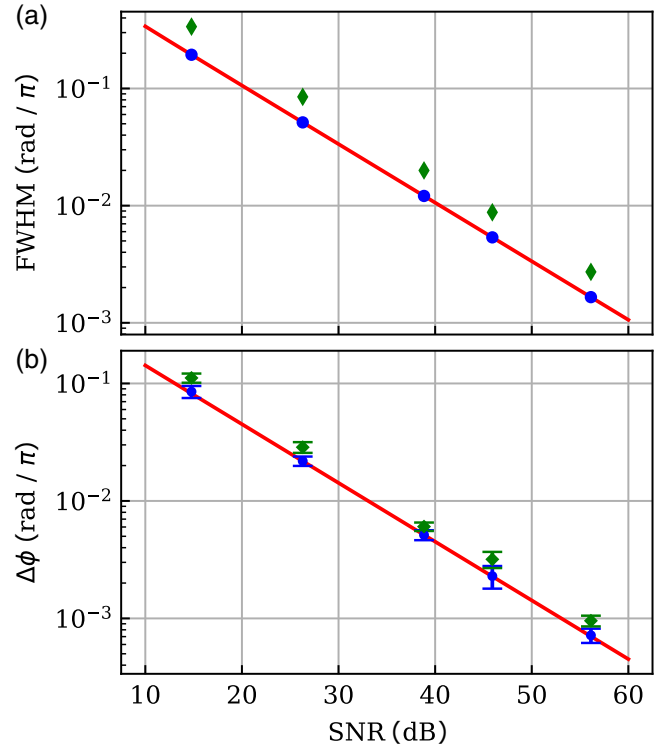


FIG. 4. (a) Phase resolution of parity measurements. Blue circles are fitted values by the maximum-likelihood method for each SNR. Green diamonds are fitted values by the threshold method with $a = 1.5\sigma$. The solid red curve is the theory that scales as $1/\sqrt{\text{SNR}}$. Errors are smaller than the symbols. (b) The minimum value of the sensitivity per phase-space measurement for the two methods. Blue circles—estimation by maximum-likelihood fit. Green diamonds—estimation by the threshold method with threshold $a = 1.5\sigma$. Dashed lines represent the corresponding theoretical curves. The solid red line is at the Cramer-Rao bound.

a factor of approximately 1.26 calculated numerically, see Appendix A 3.

V. DISCUSSION AND OUTLOOK

We have demonstrated two methods for estimating the expectation value of the parity operator, both based on the reconstruction of the Wigner representation by an effective homodyne detection. The Wigner representation reduces to the IQ distribution in this case of Gaussian states and considerable thermal noise. Thus, as the quantum and thermal fluctuations are scaled on a common footing, our work immediately extends to any domain and temperature between the quantum to classical divide.

The first method is based on a maximum-likelihood fit of the phase-space measurements to a Gaussian distribution. This method saturates the CR bound. It seems that for this method, at least two measurements are required to estimate the maximum-likelihood fit, but since the noise in the system should remain constant, it can be calibrated, and a single measurement would suffice to estimate the

current mean value of the distribution and to complete the maximum-likelihood fit. In comparison to the maximum-likelihood method, the threshold method is straightforward to implement and faster to calculate, though choosing the optimal threshold always requires calibration of the noise. The freedom of choice of the threshold parameter allows choosing a combination of the superresolution and the sensitivity, where the quality of one comes at the expense of the other. This trade-off is defined by a single parameter a/σ . Unlike the maximum-likelihood estimation method, the minimum achievable sensitivity with this method saturates the CR bound only up to a factor of approximately 1.26. Both methods can have an enhanced resolution by increasing the SNR, e.g., by increasing the integration time.

The sensitivity of a measurement describes the certainty in which the phase is estimated. It is influenced by the inherent noise in the physical state that is used for sensing, and by the dependence between the measured quantity and the estimated parameter as in Eq. (2). The resolution property is useful when it is desirable to differentiate between two settings of the measured phase. The Rayleigh limit on resolution does not depend on the SNR of the measurement, thus it lacks a key practical aspect. Using the methods presented here, the resolution scales with the SNR the same way as the sensitivity does, giving the resolution its intuitive interpretation in resolving and differentiating between settings. This work can be extended to free space with phase estimation used for refining both range and direction measurements. Further research includes significantly reducing the microwave system's inherent thermal noise by cooling parts of the setup. Using squeezed states, will result in a super-sensitivity measurement [1]. All of these extensions are also in the framework of Gaussian states.

ACKNOWLEDGMENTS

We would like to thank Dr. Lior Cohen for fruitful discussions and the support of ISF Grants No. 963.19 and No. 2323.19. L.S.'s contributions were completed while he was affiliated with the Hebrew University of Jerusalem.

APPENDIX A: DETAILED THEORETICAL BACKGROUND

For phase-sensitive measurements, the phase is estimated by measuring a parameter $M(\phi)$, which is susceptible to the phase. The width of the parameter's function with respect to the phase is the resolution of the measurement:

$$\text{Res}(\phi) = \text{FWHM}(M(\phi)). \quad (\text{A1})$$

In principle, for a noiseless measurement, when the resolution function is unambiguous and reversible over the

measurement range—we can identify the phase with infinite precision. When a phase measurement is used for imaging or direction finding, a narrow resolution function enables resolution of smaller features of the image or multiple elements. When a measurement is conducted with noise, the precision of the phase is derived from the precision of the measurement ΔM and the slope of the function $M(\phi)$:

$$\Delta\phi = \frac{\Delta M}{\partial M/\partial\phi}, \quad (\text{A2})$$

and is called the sensitivity of the measurement. Thus, to have a more sensitive measurement, one would like to measure a low noise parameter and a narrow resolution feature with a steep slope.

When the noise statistics are known, the CR bound [21,22], derived from the Fisher information of the signal, gives the maximum possible precision of the phase estimation over various measurements and estimators. The classical limit of a phase-resolution measurement is half of the used wavelength (such as the Rayleigh limit of imaging resolution), and shot noise imposes the limit for sensitivity. The new possibilities introduced by quantum mechanics to phase measurements are achieved by using states of the electromagnetic field with noise lower than the shot noise limit; using entanglement for enhancing correlations and thus signal-to-noise ratio [28–30]; and also by making measurements of quantum observables (which are also operators in the mathematical representation of quantum mechanics) [18]. One such observable is the parity operator $\hat{\Pi}$, the expectation value of which was shown to present superresolution for phase estimation using coherent states, saturating the shot noise limit when no thermal noise is present. It was also shown to exhibit super-sensitivity when using quantum two-mode squeezed vacuum (TMSV) states. The parity operator is defined as

$$\hat{\Pi} = (-1)^{\hat{N}}, \quad (\text{A3})$$

where \hat{N} is the photon-number operator. It can also be shown that the expectation value of the parity operator is the value at the origin point (0, 0) of the Wigner representation of a quantum state [31]. The Wigner representation is a quasiprobability distribution of conjugate quantum operators like position and momentum or the quadratures of the electromagnetic field. Conjugate quantum operators follow the Heisenberg uncertainty relation and thus cannot be measured simultaneously without violating the Heisenberg uncertainty principle, which gives the quantum limit of sensitivity [18,32].

In general, the Wigner representation is very different from an IQ phase diagram, as it can have negative values in restricted areas of the phase space. In addition, a point in phase space cannot be measured directly since this

violates the Heisenberg uncertainty principle. However, there are still a variety of quantum phenomena that can be observed and exploited using Gaussian states, which are states for which the Wigner representation is Gaussian and thus can be easily analyzed and measured. Those states include, for instance, coherent states, thermal states, coherent states superimposed with thermal noise, squeezed states and TMSV. The classical phase-space distribution and the Wigner representation coincide in these cases. Moreover, for room-temperature thermal noise, classically measuring the quadratures while ignoring the uncertainty principle has a negligible effect on the results. The classical and quantum Fisher information and CR bound coincide for these states as well [24].

A single mode of the electromagnetic field is similar to a harmonic oscillator with the dimensionless Hamiltonian:

$$\hat{H} = \frac{1}{2}\hat{X}^2 + \frac{1}{2}\hat{P}^2 = \hat{N} + \frac{1}{2}, \quad (\text{A4})$$

where X and P are the conjugate operators, which are the two quadratures of the electromagnetic field, following the Heisenberg uncertainty principle: $\Delta X \cdot \Delta P \geq \frac{1}{2}$ and also the more subtle $\Delta N \cdot \Delta \phi \geq \frac{1}{2}$. We present here analysis for a single-mode symmetric Gaussian state. The derivation for a general multimode Gaussian state is straightforward. The Wigner representation of a symmetric Gaussian state is

$$W(x, p) = \frac{1}{2\pi\sigma^2} \times \exp\left(-\frac{(x - \mu \cos(\theta))^2 + (p - \mu \sin(\theta))^2}{2\sigma^2}\right), \quad (\text{A5})$$

where μ is the displacement of the distribution from the origin with some predefined reference phase θ . For a coherent state $\sigma^2 = \frac{1}{2}$, is the minimum possible quantum noise that is symmetric for both quadratures. A coherent state is also a shot-noise-limited signal. $\mu^2/2 = N_c$ is the average number of photons. Most commonly, a coherent state is characterized by the complex parameter α for which $|\alpha|^2 = N_c = 2\mu^2$, its phase is the phase of the coherent signal and the displacement operator is parameterized by it [25]. We chose to work here with the definition of μ since it is more convenient when working with the Wigner representation. For a thermal state $\mu = 0$ and $\sigma^2 = N_{\text{th}} + \frac{1}{2}$, where N_{th} is the average number of photons in the thermal state. For a coherent state superimposed with thermal noise in the same frequency mode, the Wigner representation is just an appropriately scaled convolution of the Wigner representations of the two states [25,26] resulting in $\mu^2/2 = N_c$ and $\sigma^2 = N_{\text{th}} + \frac{1}{2}$. We define a

phase-space signal-to-noise ratio as

$$\text{SNR} = \frac{N_c}{N_{\text{th}} + 1/2}. \quad (\text{A6})$$

This value coincides with the full definition of signal-to-noise ratio when the thermal noise is much higher than the shot noise. For white noise such as the noise in our system, the SNR scales down linearly with increased integration time. The expectation value of the parity operator of such a Gaussian state is

$$\langle \hat{\Pi} \rangle = \sum_{n=0}^{\infty} (-1)^n \cdot P_n = \pi \cdot W(0, 0) = \frac{1}{2\sigma^2} e^{-\frac{\mu^2}{2\sigma^2}}. \quad (\text{A7})$$

P_n is the probability of measuring n photons. For an interferometric phase measurement of a coherent state with $\mu_0^2/2$ total number of photons and an interferometric phase ϕ , at the output of one interferometer arm $\mu = \mu_0 \cdot \sin(\phi/2)$, and the number of photons is

$$\mu^2/2 = N_c \cdot \sin^2(\phi/2) = \mu_0^2/2 \cdot \sin^2(\phi/2) \quad (\text{A8})$$

and the phase

$$\theta = \phi/2. \quad (\text{A9})$$

The expectation value of the parity operator thus follows:

$$\langle \hat{\Pi} \rangle = \pi \cdot W(0, 0) = \frac{1}{2N_{\text{th}} + 1} e^{-\frac{N_c \sin^2(\phi/2)}{N_{\text{th}} + 1/2}}. \quad (\text{A10})$$

From the phase-space distribution, for cases in which the SNR is large, the standard deviation of the phase can be easily calculated to be $\Delta\theta = \sigma/\mu$ by changing to polar coordinates, thus the CR bound on measuring an interferometric phase ϕ for high SNR is given by

$$\Delta\phi_{\text{min}} = 2 \frac{\sigma}{\mu_0} = \sqrt{\frac{2}{\text{SNR}}} = \sqrt{2 \frac{N_{\text{th}} + 1/2}{N_c}}, \quad (\text{A11})$$

which is reduced to the shot noise limit when $N_{\text{th}} = 0$.

1. Direct measurement of $\hat{\Pi}$

Since the parity operator is $\hat{\Pi} = (-1)^{\hat{N}}$, a direct measurement of the parity operator is possible if a photon-number measurement is available. This is achievable more easily at room-temperature environment in the optical regime, but also in the rf domain with cryogenics. In this case, its mean value could be calculated simply by ensemble averaging. The error of such a measurement is the standard deviation of the parity operator and the calculated sensitivity of the measurement is

$$\Delta\phi = \frac{\sqrt{\frac{1}{2N_{\text{th}}+1} e^{\frac{4N_c \sin^2(\phi/2)}{2N_{\text{th}}+1}} - 1}}{\left| \frac{N_c}{2N_{\text{th}}+1} \sin(\phi) \right|}. \quad (\text{A12})$$

2. Estimating $\langle \hat{\Pi} \rangle$ by maximum likelihood

A direct measurement of parity is not always available. In fact, sometimes estimating the mean value of the parity from the number of photons is better than from parity values (since the parity value has less information than the number of photons). By measuring the field quadrature distribution in phase space, the $W(0,0)$ value can be estimated using a maximum-likelihood fit. The Fisher information for estimating the mean and variance of a two-dimensional symmetric Gaussian distribution by a maximum-likelihood fit is given by

$$\mathcal{I}(\mu, \sigma^2) = \begin{pmatrix} \frac{1}{\sigma^2} & 0 \\ 0 & \frac{1}{\sigma^4} \end{pmatrix}. \quad (\text{A13})$$

Using this, the error of estimating the value at the origin, normalized to a single phase-space measurement is

$$\pi \cdot \Delta W(0,0) = \Delta \langle \hat{\Pi} \rangle = \frac{1}{2\sigma^2} e^{-\frac{\mu^2}{2\sigma^2}} \cdot \sqrt{1 + \frac{\mu^2}{\sigma^2}}. \quad (\text{A14})$$

The sensitivity of this estimation is given by

$$\Delta\phi = \sqrt{(\cot^2(\phi/2) + \left(\frac{N_{\text{th}} + 1/2}{N_c}\right)^2 \frac{2}{\sin(\phi)})}, \quad (\text{A15})$$

the minimum value of this sensitivity is given by

$$\Delta\phi_{\text{min}} = \sqrt{\frac{2}{\text{SNR}^2} + 2\sqrt{\frac{1}{\text{SNR}^2} \left(\frac{1}{\text{SNR}^2} + 1\right)}} \\ \xrightarrow{\text{SNR} \rightarrow \infty} \sqrt{\frac{2}{\text{SNR}}},$$

which reduces to the CR bound for large values of SNR.

3. Estimating $\langle \hat{\Pi} \rangle$ by threshold analysis

Another method for estimating $W(0,0)$ [15,16] would be an approximation to a projection measurement on $W(0,0)$. For a photon-number measurement, this would be a projection on the vacuum state, measuring the probability that no photons arrived at all. For a phase-space measurement, this would be done by calculating the probability of the measurement being inside some phase-space area defined by a threshold radius a from the origin:

$$\tilde{W}(0,0) \approx \frac{1}{\pi a^2} \int_0^{2\pi} d\theta \int_0^a dr r W(r,\theta). \quad (\text{A16})$$

The probability of the measurement being inside this radius is given by the cumulative distribution function (CDF) of the marginal radial distribution in the phase

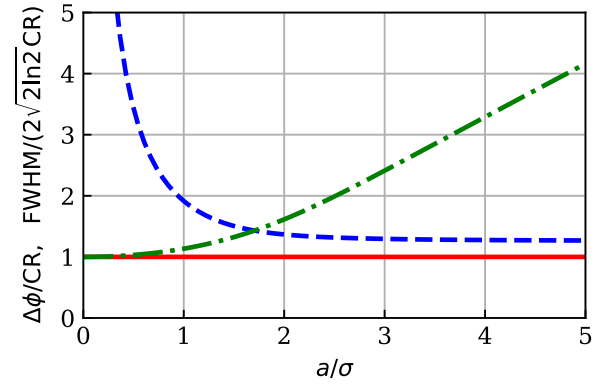


FIG. 5. Resolution and sensitivity as a function of the threshold a . Green dot-dashed line represents resolution, and blue dashed line is for the sensitivity. Solid red line represents the Cramer-Rao bound. The x axis is normalized per standard deviation of the noise σ , and the y axis is per one CR bound.

space up to a . For a symmetric Gaussian distribution, the marginal radial distribution is Rician. The smaller the threshold, the better the estimation in the limit of many measurements, but a larger number of measurements would be required. The choice of the threshold radius a also defines different performance attributes for resolution and sensitivity. Figure 5 shows the trade-off between resolution and sensitivity for different values of a . This plot is universal when a is normalized to σ (defined by the noise) and when the sensitivity is normalized to the CR bound (defined by the SNR). The resolution here is normalized to $2\sqrt{2\ln 2}$ times the CR bound. This factor relates the resolution defined by FWHM in contrast to the sensitivity defined by standard deviation. With this normalization, the trade-off between resolution and sensitivity could be better appreciated. The minimum possible resolution with this method matches that of the maximum-likelihood method. However, the minimum possible sensitivity does not saturate the CR bound but asymptotically reaches it up to a factor of approximately 1.26, which was calculated numerically. The balance point of similar performance of both resolution and sensitivity is at $a/\sigma \approx 1.7$.

This threshold method is a projection measurement or a Bernoulli trial with two outcomes. One of them is the probability of having a sample inside the radius a , which resembles the estimate of $\langle \hat{\Pi} \rangle$ given by Eq. (A16)

$$p = \int_0^{2\pi} d\theta \int_0^a dr r W(r,\theta). \quad (\text{A17})$$

Using this equation, we can calculate the resolution for a given phase-space distribution. The error in calculating the Bernoulli probability p is just $\Delta p = \sqrt{p}$ per phase-space sample point (and is reduced as the square of the number of sample points) and so the sensitivity can be calculated. A different combination of resolution and sensitivity for

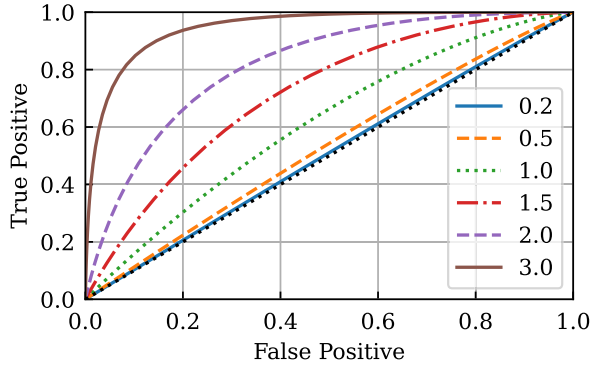


FIG. 6. ROC curve for several acceptable deviations (ADs) in units of the Cramer-Rao bound. From straight to curved, the curves correspond to $0.2AD/CR$ (blue) up to $3AD/CR$ (brown). Each curve is parametrized by the detection threshold a/σ . In these normalized units, the figure is universal.

different applications might be useful. For a given N_c and N_{th} , which define the distribution, it is possible to choose the best working point in terms of combined resolution and sensitivity, as shown in Fig. 5. Another performance analysis can be made for applications in which phase locking is required. For such applications, one needs to define the precision within which one wants to be locked. Suppose one wants to be locked on the phase to within an acceptable deviation (AD) $\Delta\phi_l$ from perfect locking. This gives us two binary thresholds. $\Delta\phi_l$ is the locked-unlocked binary threshold for the true state of the system and a in a binary threshold of our estimation. Now we can calculate the probabilities of actual conditions versus predicted conditions. For example, in radar applications, it is common to plot a receiver operating characteristic (ROC) curve, which is the true-positive alerts versus false-positive alerts probabilities. In our case, a true-positive occurrence is when $\phi < \Delta\phi_l$ and we received a sample within the threshold a . A false-positive occurrence is when $\phi > \Delta\phi_l$ but we still received a sample within the radius a . Figure 6 shows parametric ROC curves for various values of locking precision $\Delta\phi_l$ parametrized with the detection threshold a . The locking precision is stated in terms of the CR bound. When a is stated in terms of σ this is a universal plot. Figure 6 is another tool to choose a working point for the threshold method.

APPENDIX B: CONTROLLING THE SNR BY INTEGRATION TIME

The FWHM of $\langle\hat{\Pi}\rangle$ follows $1/\sqrt{SNR}$ scaling. The different SNR values in the main paper were achieved by controlling the signal power with a constant integration time of 25 ns. Higher SNR and higher resolution can also be obtained by a longer integration time with constant signal power. When considering the energy within

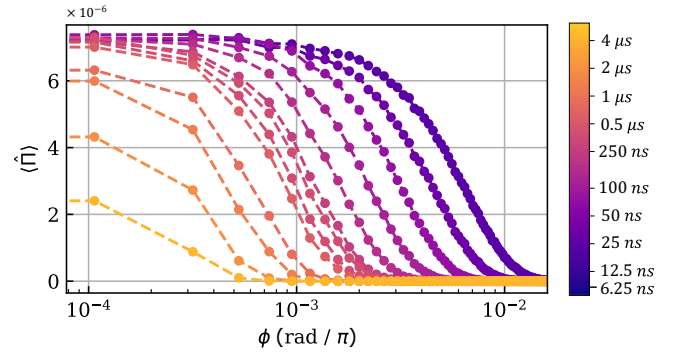


FIG. 7. Resolution feature of $\langle\hat{\Pi}\rangle$ using the maximum-likelihood method for different integration times at $SNR = 45.9$ dB. As the integration time grows, first the width is just reduced as the SNR increases. At a certain point, the noise becomes comparable to the remaining signal power due to the imperfect extinction ratio, and the height of the feature is reduced as well.

a certain integration time, N_c increases linearly with integration time, however N_{th} does not change. This happens due to the fact that the frequency mode of the photons is defined up to the inverse of integration time, thus when the integration time grows, the overall average noise energy increases linearly but the bandwidth of the mode decreases linearly leaving N_{th} , the overall average number of photons in the mode, constant (since the thermal noise is white). We can also analyze the system in units of power, treating N_c and N_{th} as the average number of photons per second. In this case, N_c does not change with the integration time but rather N_{th} decreases linearly since it is normalized per a certain time interval. The quadrature noise in this case scales as \sqrt{Hz} . The overall effect, however, does not change since the SNR changes in the same way in both pictures.

Increasing the integration time is limited in practice by the setup's extinction ratio, which was 90 dB in our setup. Such a high extinction ratio was achieved by controlling the losses in both arms of the interferometer and minimizing the dark port output power. The resolution feature of $\langle\hat{\Pi}\rangle$ for several integration times with constant power is shown in Fig. 7. Ideally, increasing the integration time results only in narrowing the resolution, and the desired SNR can be achieved with longer integration times. However, when the noise of the distribution becomes comparable to the leakage power in the interferometer due to the imperfect extinction ratio, it lowers the maximum value of the resolution feature and reduces the quality of the measurement.

Figure 8 shows $\langle\hat{\Pi}\rangle$ as estimated by a maximum-likelihood fit for several values of signal power at a constant integration time of 25 ns. It is plotted with logarithmic x axis, which shows clearly the dependence of the resolution width on SNR.

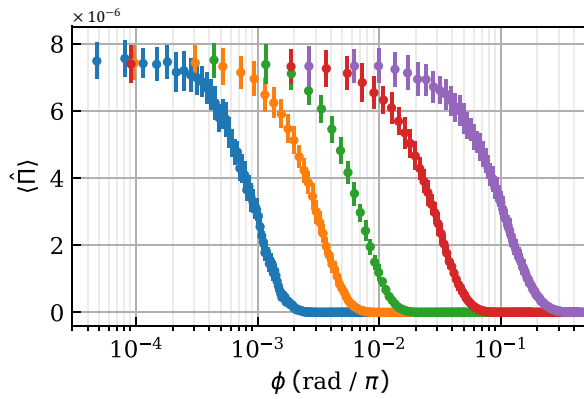


FIG. 8. Parity calculated using the maximum-likelihood method with logarithmic x axis, the width scales linearly with the SNR.

- [1] Min Xiao, Ling-An Wu, and H. J. Kimble, Precision measurement beyond the shot-noise limit, *Phys. Rev. Lett.* **59**, 278 (1987).
- [2] J. Aasi, *et al.*, Enhanced sensitivity of the LIGO gravitational wave detector by using squeezed states of light, *Nat. Photonics* **7**, 613 (2013).
- [3] Nicolas Didier, Archana Kamal, William D. Oliver, Alexandre Blais, and Aashish A. Clerk, Heisenberg-limited qubit read-out with two-mode squeezed light, *Phys. Rev. Lett.* **115**, 093604 (2015).
- [4] A. Bienfait, P. Campagne-Ibarcq, A. H. Kiielerich, X. Zhou, S. Probst, J. J. Pla, T. Schenkel, D. Vion, Daniel Estève, J. J. L. Morton, *et al.*, Magnetic resonance with squeezed microwaves, *Phys. Rev. X* **7**, 041011 (2017).
- [5] Yoad Michael, Leon Bello, Michael Rosenbluh, and Avi Pe'er, Squeezing-enhanced Raman spectroscopy, *npj Quantum Inf.* **5**, 81 (2019).
- [6] Jonathan P. Dowling, Quantum optical metrology—the lowdown on high-NOON states, *Contemp. Phys.* **49**, 125 (2008).
- [7] Yonatan Israel, Shamir Rosen, and Yaron Silberberg, Supersensitive polarization microscopy using NOON states of light, *Phys. Rev. Lett.* **112**, 103604 (2014).
- [8] Naeimeh Mohseni, Shahpoor Saeidian, Jonathan P. Dowling, and Carlos Navarrete-Benlloch, Deterministic generation of hybrid high- n NOON states with Rydberg atoms trapped in microwave cavities, *Phys. Rev. A* **101**, 013804 (2020).
- [9] M. D. Mazurek, K. M. Schreiter, R. Prevedel, R. Kaltenbaek, and K. J. Resch, Dispersion-cancelled biological imaging with quantum-inspired interferometry, *Sci. Rep.* **3**, 1582 (2013).
- [10] R. Kaltenbaek, J. Lavoie, D. N. Biggerstaff, and K. J. Resch, Quantum-inspired interferometry with chirped laser pulses, *Nat. Phys.* **4**, 864 (2008).
- [11] Xiao-Jie Tan, Luo Qi, Lianwei Chen, Aaron J. Danner, Pakorn Kanchanawong, and Mankei Tsang, Quantum-inspired superresolution for incoherent imaging, *Optica* **10**, 1189 (2023).
- [12] Yoann Altmann, Stephen McLaughlin, Miles J. Padgett, Vivek K. Goyal, Alfred O. Hero, and Daniele Faccio, Quantum-inspired computational imaging, *Science* **361**, eaat2298 (2018).
- [13] Kwan Kit Lee, Christos N. Gagatsos, Saikat Guha, and Amit Ashok, Quantum-inspired multi-parameter adaptive Bayesian estimation for sensing and imaging, *IEEE J. Sel. Top. Signal Process.* **17**, 491 (2023).
- [14] Mark Moore and Ajit Narayanan, *Department of Computer Sciences* (University Exeter, Exeter, UK, 1995).
- [15] L. Cohen, D. Istrati, L. Dovrat, and H. S. Eisenberg, Super-resolved phase measurements at the shot noise limit by parity measurement, *Opt. Express* **22**, 11945 (2014).
- [16] Emanuele Distante, Miroslav Ježek, and Ulrik L. Andersen, Deterministic superresolution with coherent states at the shot noise limit, *Phys. Rev. Lett.* **111**, 033603 (2013).
- [17] Kebei Jiang, Hwang Lee, Christopher C. Gerry, and Jonathan P. Dowling, Super-resolving quantum radar: Coherent-state sources with homodyne detection suffice to beat the diffraction limit, *J. Appl. Phys.* **114**, 193102 (2013).
- [18] Petr M. Anisimov, Gretchen M. Raterman, Aravind Chiruvelli, William N. Plick, Sean D. Huver, Hwang Lee, and Jonathan P. Dowling, Quantum metrology with two-mode squeezed vacuum: Parity detection beats the Heisenberg limit, *Phys. Rev. Lett.* **104**, 103602 (2010).
- [19] William N. Plick, Petr M. Anisimov, Jonathan P. Dowling, Hwang Lee, and Girish S. Agarwal, Parity detection in quantum optical metrology without number-resolving detectors, *New J. Phys.* **12**, 113025 (2010).
- [20] Q. Wang, L. Hao, Y. Zhang, C. Yang, X. Yang, L. Xu, and Y. Zhao, Optimal detection strategy for super-resolving quantum lidar, *J. Appl. Phys.* **119**, 023109 (2016).
- [21] C. Radhakrishna Rao, in *Breakthroughs in Statistics: Foundations and Basic Theory*, edited by S. Kotz and N. L. Johnson (Springer New York, New York, NY, 1992), p. 235.
- [22] C. L. Degen, F. Reinhard, and P. Cappellaro, Quantum sensing, *Rev. Mod. Phys.* **89**, 035002 (2017).
- [23] In units of $\hbar = 1$.
- [24] O. Pinel, P. Jian, N. Treps, C. Fabre, and D. Braun, Quantum parameter estimation using general single-mode Gaussian states, *Phys. Rev. A* **88**, 040102 (2013).
- [25] Roy J. Glauber, Coherent and incoherent states of the radiation field, *Phys. Rev.* **131**, 2766 (1963).
- [26] Myung Shik Kim and Nobuyuki Imoto, Phase-sensitive reservoir modeled by beam splitters, *Phys. Rev. A* **52**, 2401 (1995).
- [27] D. M. Pozar, *Microwave Engineering* (Wiley, 2011).
- [28] Seth Lloyd, Enhanced sensitivity of photodetection via quantum illumination, *Science* **321**, 1463 (2008).
- [29] S. Barzanjeh, S. Pirandola, D. Vitali, and J. M. Fink, Microwave quantum illumination using a digital receiver, *Sci. Adv.* **6**, eabb0451 (2020).
- [30] Jeffrey H. Shapiro, The quantum illumination story, *IEEE Aerosp. Electron. Syst. Mag.* **35**, 8 (2020).
- [31] William B. Case, Wigner functions and Weyl transforms for pedestrians, *Am. J. Phys.* **76**, 937 (2008).
- [32] Holger F. Hofmann, All path-symmetric pure states achieve their maximal phase sensitivity in conventional two-path interferometry, *Phys. Rev. A* **79**, 033822 (2009).